Chapter 12

Application of Liquid Laser Ablation: Organic Nanoparticle Formation and Hydrogen Gas Generation

Ikuko Akimoto and Nobuhiko Ozaki

Additional information is available at the end of the chapter

http://dx.doi.org/10.5772/64939

Abstract

Laser ablation is induced by a heating process of materials through the absorption of laser light and results in an explosive expansion of materials. For materials located in liquid, in contrast to those in vacuum, laser ablation proceeds under rather mild conditions via a cycle of heating and cooling by mediated solvent; therefore, it is applicable for organic solids to fragment into nanoparticles. Alternatively, for effective light absorbers, the irradiated site becomes the reaction centre of a photochemical reaction even in liquids, resulting in hydrogen gas generation. In this chapter, two topics of laser ablation in the liquid phase are presented: nanoparticle formation of organic materials and hydrogen gas generation from solid carbon in water. Thereby, the extended abilities of liquid laser ablation to transform ordinary materials into functional ones are introduced.

Keywords: organic nanoparticles, colloidal solution, hydrogen generation, carbon-based nanoparticles, spectroscopy, nanosecond laser pulses

1. Introduction

Laser ablation in the liquid phase, which is a breakdown method leading to nanoparticle formations developed in the study of laser-processing techniques using short and ultrashort laser pulses [1, 2], was applied to organic materials in the middle of the 1990s by Masuhara and coworkers [3–14]. In the liquid phase, laser ablation proceeds under rather mild conditions via a cycle of heating by light absorption and cooling by mediated solvent molecules under ambient atmospheric pressure and temperature, in contrast to the laser ablation in the gas phase such as

laser deposition of metals under vacuum [2]. Therefore, it is applicable for an organic material that is more intolerant of optical radiation than a metal or an inorganic semiconductor.

Laser ablation of an organic material in the liquid phase results in impressive phenomena. Microcrystals of an organic material suspended in a poor solvent, typically water, are irradiated by laser pulses; thereby, the cloudy suspension is transformed into transparent-colored water. The resultant is a colloidal solution containing organic fragments of a few tens to hundreds nanometers in diameter, that is, nanoparticles. The colloidal solution is stable for a long time without any surfactants, typically for weeks or more, because of persistent Brownian motion of the nanoparticles in the solvent [12]. Therefore, laser ablation in the liquid phase produces a uniform solution of small organic materials. The size of the nanoparticles can be controlled by the ablation conditions such as the irradiated laser fluence [15], laser pulse duration [16], and wavelength [10]. The easy and high collectability of the created nanoparticles by treating the solution is a useful characteristic of laser ablation in the liquid phase.

Such a colloidal solution is applicable in an ink print, a drag delivery, and cosmetic applications. In particular, it is expected to provide a low-cost wet process in the device fabrication field. In recent years, organic materials are increasingly utilized in optical and electronic devices such as organic light-emitting diodes (OLEDs) [17] and organic field-effect transistors (OFETs) [18]. However, high-cost vacuum sublimation processes are required for the fabrication of such devices, because small organic molecules are difficult to dissolve in solvents without the addition of hydrophilic moieties on the molecule or any surfactants. The attachment of additional moieties generally does not guarantee the original functions of molecules, and surfactants may affect the functions of systems. Therefore, the formation of a stable solution of the target organic materials by laser ablation is a promising technique for the device fabrication. The colloidal solution gives a significant advantage to the industrial field with regard to low-cost and eco-friendly products, by applying a print technique as introduced in Ref. [19].

Alternatively, an irradiated site in laser ablation can be a reaction centre of photochemistry for energy conversion from light to a fuel gas. A novel hydrogen generation method was discovered during laser ablation of solid carbon in water [20, 21]. Hydrogen gas is a clean gaseous fuel, and hydrogen generation methods have been intensively studied. Classical coal gasification [22] and optically induced water-splitting in the presence of a photocatalyst titanium oxide [23] are representative phenomena in hydrogen generation methods. In the photocatalytic water-splitting reaction, the addition of solid carbon assisted the reaction by avoiding the reverse reaction through oxidization [24, 25]. Thus, solid carbon has been utilized for hydrogen gas production. However, the optical activity of solid carbon itself was not known before the discovery.

As by-products of this laser-induced hydrogen gas generation reaction, nanoparticles of carbon-based materials were also found in the post-irradiated solution. Thus far, novel carbon-based materials, such as graphene oxide (GO) [26–28], nano-diamond [29, 30], and diamond-like carbon (DLC) [29, 31], have been studied as photocatalysts in the water splitting reaction [26, 30] and reduction of carbon oxide [27, 28]. These carbon-based materials can be produced by laser ablation of solid carbon as demonstrated in Refs. [29, 31]. Therefore, laser ablation of

solid carbon in an aqueous solution is attractive for at least two different interests: hydrogen generation and carbon-based nanoparticle production.

In this chapter, two topics of laser ablation in the liquid phase using nanosecond laser pulses are presented. The first is nanoparticle formation of organic materials, particularly from the points of particle size control by irradiated laser fluence and absorption spectrum properties depending on particle size. The second is hydrogen gas generation from solid carbon in water accompanied with nanoparticle generation. Through these topics, the extended abilities of liquid laser ablation to transform ordinary materials into functional ones are introduced.

2. Laser ablation techniques

2.1. Procedure of laser ablation in the liquid phase

Laser ablation in liquid phase is performed for a solid material suspended in poor solvent, in which the material is difficult to dissolve, by irradiation of laser pulses through the side wall of a transparent cuvette/bottle or the top surface of the solution. The suspension was stirred by a magnetic stirrer during the irradiation. The experiments presented in this chapter were performed with laser pulses of 5 ns pulse duration from a tunable optical parametric oscillator excited by a Q-switched YAG laser operated at a 10 Hz repetition rate (Spectra Physics, MOPO) or from a second harmonics of a Q-switched YAG laser (Continuum Surelite) operated at a 10 Hz repetition rate. The incident laser power was controlled using a Glan-Laser calcite polarizer. By maintaining the laser beam unfocused or loosely focused, the energy density was maintained below a few hundred milli-joule per square centimeter in order to not achieve a plasma state [29, 32, 33]. The experimental details are described in the following sections. All laser ablation experiments were performed at room temperature (24°C).

2.2. Nanoparticle formation for organic molecules in water

Laser ablation of organic molecules was performed with dispersed mixture of organic molecules in the distilled water in quartz cuvette of $1 \times 1 \times 5$ cm^3 at a concentration in the range from 2×10^{-2} to 5×10^{-5} mol/l. The microcrystals in suspension were irradiated by laser pulses for a few minutes. The wavelengths of the irradiated laser pulse were selected corresponding to absorption band of molecules. Here, results for two materials are presented; a yellow pigment quinacridone quinone (QQ, Aldrich) was irradiated at the wavelength 430 nm, and rubrene (Rb, Aldrich, sublimated grade) was irradiated at 520 nm. More details of preparation procedure were described in Refs. [34, 35].

Post-irradiated solution was investigated by UV-VIS absorption measurement with a conventional system (JASCO, V-560) and a dynamic light scattering (DLS) measurement (HORIBA Scientific, nanopartica, or Otsuka Electronics, Photal). The mode diameter, which indicates the most frequent diameter of nanoparticles in the ensemble, was employed to estimate the size of particles. Dried nanoparticles in deposited films were visualized by an atomic force microscopy (AFM) (SII, SPA400) and the transmission electron microscopy (TEM) (JEOL,

2000EX). Surface electric potential on the nanoparticles was obtained by a ζ-potential measurement (HORIBA Scientific, nanopartica, or Otsuka Electronics, Photal). A film of the QQ nanoparticles was prepared on a glass substrate covered by an indium-tin-oxide (ITO) transparent electrode by the electrophoretic deposition (EPD) method, and its UV-VIS absorption spectrum was compared with that of a vapor-deposited film of QQ with a thickness of 46.5 nm and that of solutions.

Time-resolved EPR measurement was carried out in QQ 2-methyltetrahydrofuran solution at 90 K and C_{60} toluene solutions at 100 K by the excitation at 430 and 532 nm, respectively, with an instrument (Bruker, ELEXSYS E580).

2.3. Gas generation via laser ablation of carbon materials in aqueous solution

In the laser ablation of carbon in aqueous solution, binchotan charcoal powder of a mean diameter 5 μm (A, Latest Coop., Wakayama, Japan), high-grade carbon powder of a mean diameter 5 μm (B, SEC, SCN-5, 99.5%), and graphite powder of a mean diameter less than 45 μm (C, Wako, 072-03845) were used. Surface area of powder was measured by the BET method developed by Brunauer, Emmett, and Teller. The mixture of the powder and distilled water was irradiated by an unfocused beam (6.2 mm in diameter) of laser pulses for 30 or 60 min. The wavelengths of the laser pulses were selected in the VIS-near-infrared (NIR) region. The generated gas was collected by the water displacement method. The collected gas volume was measured with a scale on a tube at a resolution of 0.05 mL.

Gas components were analyzed by quadrupole mass spectrometry (Nuclear Engineering Co., Ltd., Ibaraki, Japan) for gases generated under argon atmosphere. The gas components were compared with two gas samples generated from binchotan powder in 100% distilled water and in 50% ethanol aqueous solution. The portion of molecules N_2, CO, and C_2H_4 of the same molecular mass at 28 was determined by filtered partial presser measurements and mass fragments at N and C in quadrupole mass spectrometer. More details of preparation procedure were described in Refs. [20, 21].

During the hydrogen generation, optical radiation from the irradiated site was observed for a commercial binchotan charcoal block and a carbon electrode block (99.9%) in distilled water (H_2O) or in 50% ethanol aqueous solution ($EtOH/H_2O$). The block was irradiated by loosely focused nanosecond laser pulses (5 ns, 10 Hz, 532 nm) with a laser beam size of 0.50 × 0.25 cm^2. The emission spectrum was detected using an intensified charge-coupled device (ICCD) (Roper Scientific, PI-MAX) attached to a monochromator (Acton, 300i) with 4 nm spectral resolution. Strong light scattering was blocked by a super notch filter designed for 532 nm incident light. More details of preparation procedure were described in Ref. [36].

Post-irradiated solutions and ablation products were investigated by UV-VIS, DLS, and TEM methods, similar to the organic nanoparticles as mentioned in Section 2.2. In addition, FT-IR spectrum of dried carbon-based nanoparticles deposited on a pure silicon substrate was observed.

http://dx.doi.org/10.5772/64939

3. Organic nanoparticle formation

The validity of the laser ablation in the liquid phase for nanoparticle generation has been demonstrated by several groups for organic systems including poly-diacetylene (poly-DCHD) [4], metallo-phthalocyanines [6–9], dendronized perylenediimide (DPDI) [13, 14], perylene [12], pentacene [37], and a series of pigments including quinacridone (QA) [10–12] and its derivatives [34, 35]. Fullerene C_{60} was also fragmented into nanoparticles by laser ablation in water [15], although it is an inorganic molecule. The number of molecules is rather limited. The diversity of applicable organic molecules for fragmentation by laser ablation is limited by the photodegradation of a molecule [34] even under the mild conditions in the liquid phase. As a result, the optical properties of the colloidal solutions need case by case interpretations. Further investigation is required for nanoparticle formation of various organic molecules by laser ablation.

The most successful organic system for laser ablation is a class of pigments, QA, and quinacridone-quinone (QQ), whose molecular structures are shown in **Figure 1**. They exhibit an excellent tolerance for photolysis. A yellow pigment QQ has a simple monomorphism crystal phase [38], which made spectral analysis easy. On the other hand, a red pigment QA has polymorphism in α, β, or γ forms, and significant spectral change was observed depending on the crystal form [10]. Therefore, QQ is more suitable to investigate the optical properties of colloidal solutions. Here, the size-dependent optical properties of the QQ colloidal solutions prepared by laser ablation in the liquid phase are presented.

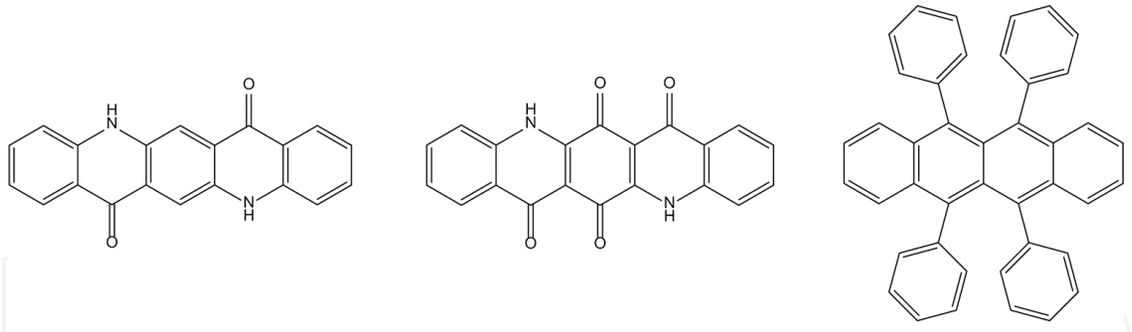

Figure 1. Molecular structures of QQ, QA, and rubrene (Rb).

3.1. Nanoparticle generation: in the case of quinacridone quinone

Figure 2a shows the absorption spectra of the supernatants before and after laser irradiation at the irradiation fluence of 11 mJ/cm^2 and the wavelength 430 nm [35]. Light extinction in the suspension is due to the absorption and scattering of light. For prolonged laser irradiation, a characteristic absorption peak at 2.88 eV increased and a scattering tails at 2.24 eV decreased. Such changes were accompanied with a visible disappearance of precipitants and appearance of a transparent yellow solution. This visible change is a characteristic of laser ablation in the

liquid phase, caused by converting precipitants to QQ nanoparticles, as described in the following section. The transparency is maintained for months, imparting interests for various applications [19].

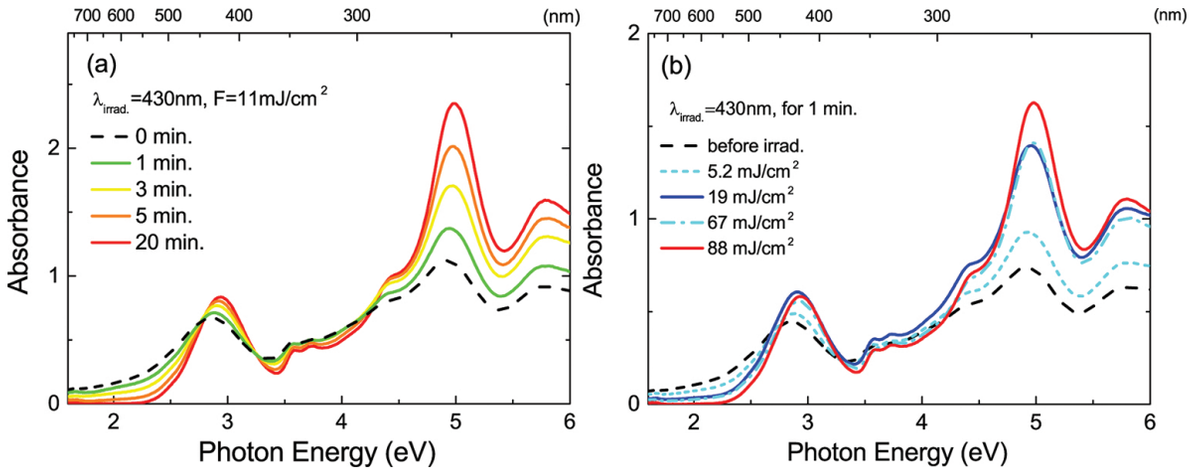

Figure 2. (a) Absorption spectra before and after various irradiation times at a laser fluence of 11 mJ/cm^2. (b) Absorption spectra before and after 1 min irradiation at various laser fluences of 5.2, 19, 67, and 88 mJ/cm^2. Adapted with permission from Ref. [35].

A similar change was also observed for increase in the irradiated laser fluence. **Figure 2b** shows the absorption spectra of the QQ supernatants before and after laser irradiation for 1 min at laser fluences of 5.2, 19, 67, and 88 mJ/cm^2. As the laser fluence increased, the absorbance increased. In addition, the peak energy clearly shifted to the higher energy side (blueshift), and each full width at half maximum (FWHM) became narrower (see **Figure 4a**). Similar spectral changes were observed above a threshold fluence, which depends on the specimens for QA in water [10], QQ in chloroform, and others [7, 14], whereas the threshold was smeared for QQ in water due to the relatively higher solubility in water [35]. Furthermore, in the case of QQ, nanoparticle generation by laser ablation was confirmed even in pH-controlled water from 2.5 to 10 by ion-exchange resin.

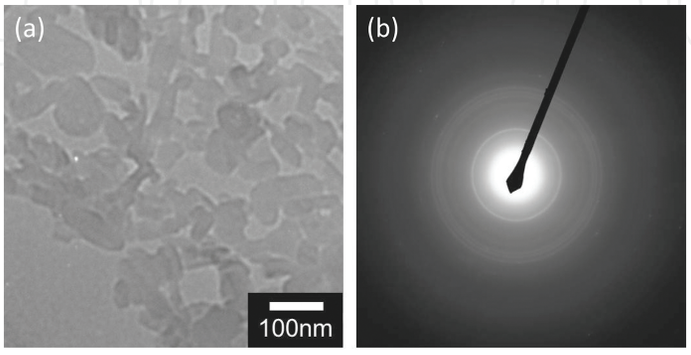

Figure 3. (a) Typical TEM image and (b) electron diffraction pattern of QQ nanoparticles prepared with the laser fluence 19.2 mJ/cm^2 for 1 min. Adapted with permission from Ref. [35].

http://dx.doi.org/10.5772/64939

The formation of nanoparticles was confirmed by AFM and TEM images of dried specimens as well as by DLS measurements of the solution. A typical TEM image of the QQ nanoparticles, which was prepared at a fluence of 19.2 mJ/cm^2 for 1 min, indicates the shape of distorted ellipsoid dispersed uniformly, as shown in **Figure 3a**. The image of the nanoparticles was observed typically in size around 90 nm, which is not far from the mode diameter observed by the DLS (78 nm). An electron diffraction pattern of the nanoparticle ensemble shows multiple Debye-Scherrer rings (**Figure 3b**), which means that the nanoparticles consist of a crystalline structure. The lattice spacings were coincident with those obtained by X-ray diffraction measurements for the QQ powder within analytical accuracy. Therefore, the crystalline structure of the QQ powder is maintained after the laser ablation in water.

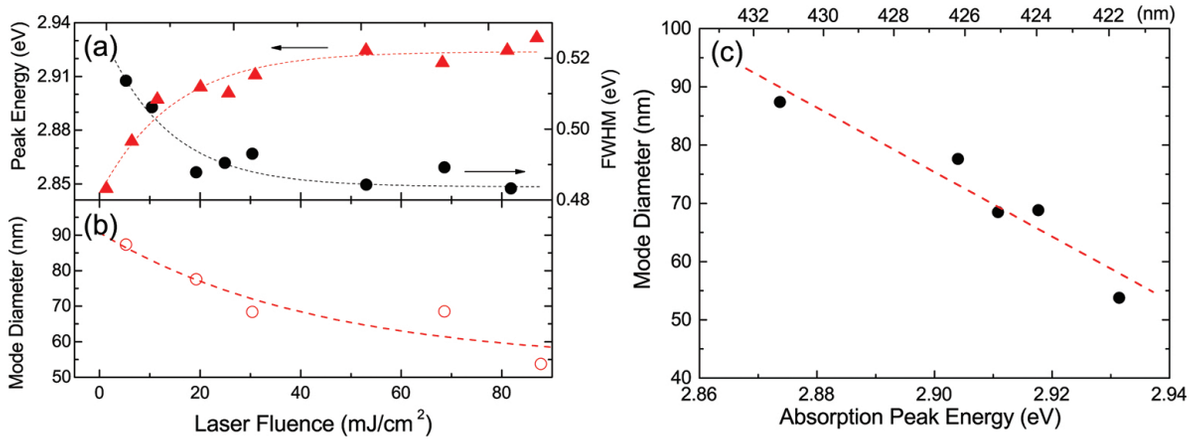

Figure 4. (a) Fluence dependence of the lowest absorption peak energy (solid triangles) and its FWHM (solid circles). (b) Fluence dependence of the mode diameter estimated by DLS (open circles). Dotted curves are guides for eyes. (c) Correlation of the mode diameter to the lowest peak energy obtained at various fluences (solid circles). A broken line is a fitting curve obtained by the least squares method. Adapted with permission from Ref. [35].

Note the relationship between the blueshift of the lowest absorption peak energy and the mode diameters of the nanoparticles contained in the solutions estimated by DLS. As shown in **Figure 4b**, the observed mode diameter was smaller for the irradiation at higher laser fluences. A linear correlation between the mode diameters and the lowest absorption peak energies was found as shown in **Figure 4c**. This relationship provides us the possibility of simple estimation of the most frequent nanoparticle diameter in an ensemble by observation of the absorption peak energy, at least, within the range from 55 to 90 nm in QQ. Such a size dependence was hidden by spectral variation due to polymorphism in QA [10] and by superposition of light scattering in DPDI [14].

The size dependence of the energy shift in the absorption spectrum can be considered in relation to the surface states. The ratio of a surface area (S) to a particle volume (V) is larger for smaller particles with the dependence of S/V=6/D, where D is the diameter. Thus, the larger shifts with the smaller particles imply influences from surface states. Indeed, the QQ nanoparticles were under a negative surface potential (ζ-potential) of −69 to −44 mV [34] in water, indicating the creation of charge or polarization on the surface by laser irradiation.

Furthermore, by utilizing the negative ζ-potential on the nanoparticles, a film was fabricated on an ITO glass electrode from the colloidal solution by electrophoretic deposition (EPD). As shown in **Figure 5**, the absorption spectrum of the nanoparticle film (d) showed that the lowest energy peak was apparent at the same position as that in the colloidal solution (c) but was shifted from those of a vapor-deposited film (b) and solution before irradiation (a) [34]. The characteristic of the colloidal solution formed by liquid laser ablation was maintained in the EPD film. A preliminary device with nanoparticles by the EPD method was demonstrated for QA [11]. Such negative surface potential response to the electric field is also applicable for the roll-to-roll fabrication method [39].

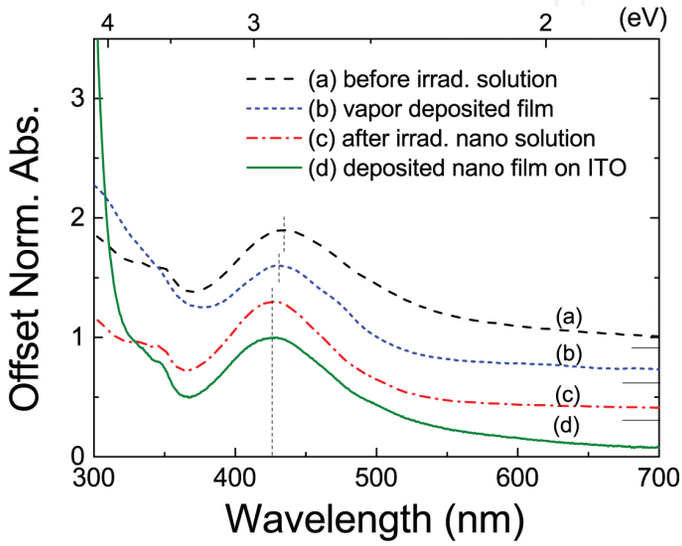

Figure 5. Comparison of normalized absorption spectra of (a) a starting aqueous QQ solution before irradiation, (b) a vapor-deposited film, (c) a colloidal solution before preparing an EPD deposit film, and (d) an EPD deposit film on an ITO electrode. Adapted with permission from Ref. [34].

3.2. Suitable organic materials for nanoparticle generation by laser ablation

No signal of photodegradation appeared in the yellow pigment QQ under the aforementioned irradiation conditions. The rigid molecular structure and stacking of flat molecules in QQ and QA systems enhance the tolerance for laser irradiation [38]. In contrast, the laser ablation of fragile and luminous molecules, such as rubrene (Rb) whose molecular structure is shown **Figure 1**, failed because Rb underwent photodissociation upon irradiation by the laser pulses [34].

Besides a molecular structure, it is worth taking into account the relaxation processes after optical excitation in order to understand the necessary condition for laser fragmentation. Because the fragmentation of organic powders into nanoparticles proceeds by rapid photo-thermal conversion on the surface layers of a solid [10], non-radiative relaxation processes, such as intersystem crossing and/or internal conversions, are potential thermal sources in the molecules. Population into an excited triplet state is a plausible entrance of the de-excitation path into thermal energy generation.

http://dx.doi.org/10.5772/64939

The population of an excited triplet state was observed for QQ and C_{60} by transient EPR measurements as shown in **Figure 6**; however, it was unobservable for Rb. Transient microwave signals of emission and absorption decayed with a lifetime of 57 μs in the QQ solution at 90 K and 3–6 μs in the C_{60} solution at 100 K, respectively. These signals arise from transitions between sublevels of an excited triplet state which were populated via efficient intersystem crossing from an excited singlet state after optical excitation. Although the observed lifetime in the C_{60} solution was much faster than the value in literature [40] due to oxidation and a high concentration of the solution, a large intersystem crossing and triplet population were obvious. Therefore, a sufficient population of an excited triplet state is one possible necessary condition for laser fragmentation via photothermal conversion in organic materials. In addition, photoluminescence (PL) from QQ was hardly observed, similar to C_{60}, in which PL was somewhat observed with a radiative quantum yield of 10^{-4} [41]. The absent of PL may also be a good signal for proceeding with the photothermal conversion.

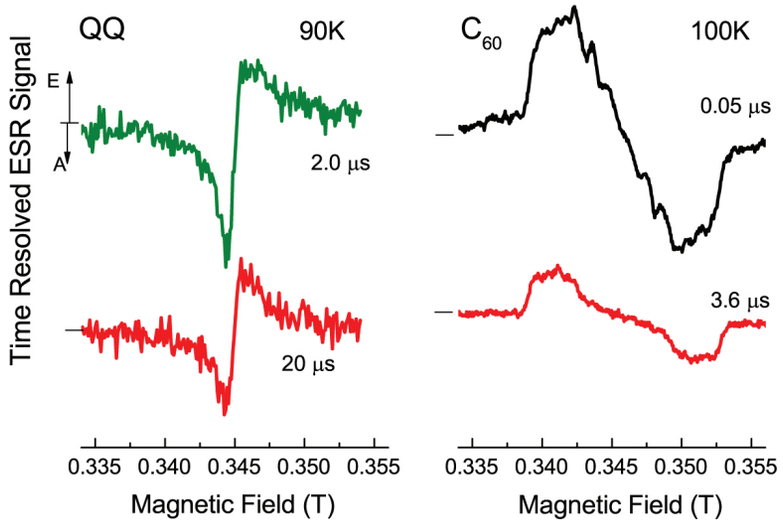

Figure 6. Time-resolved EPR signals for a QQ solution at 90 K and electron-spin-echo-detected time-resolved EPR signals for the C_{60} solution at 100 K.

4. Hydrogen generation

From another viewpoint, the irradiated site in the laser ablation can be a reaction centre of energy conversion from light to a fuel gas. In this section, our recent discovery of novel hydrogen gas generation during laser ablation of carbon in an aqueous solution [20, 21] is presented. This reaction proceeded via a photochemical reaction that carried the temperature elevation of the irradiated sites in water [36]. Electrodes and any other photocatalysts were not necessary for such reactions. Furthermore, the hydrogen generation was accompanied by simultaneous carbon-based nanoparticle production. Therefore, the laser ablation of carbon in water demonstrated two different interests: the hydrogen generation and the carbon-based nanoparticle production.

This hydrogen generation reaction occurred under a lower irradiation energy than that required for plasma-state generation. It has been known that the plasma state is induced when the laser pulse energy is focused on materials with an energy density over a few joule per square centimeter [29, 32]. Such an exploded plasma gas is the result of material dissociation and has been investigated, for example, in laser-induced breakdown spectroscopy (LIBS) by measuring the luminescence from the plasma state [29, 32]. In contrast, in the present reaction, no evidence of a plasma state was observed, but temperature elevation at the irradiated site was confirmed by spectroscopy [36] as described in Section 4.5.

In this reaction, a high-grade Japanese charcoal, known as binchotan in Japan, is adopted as the carbon source because of its high carbonization over 93%. Among various carbon materials, charcoal is a sustainable carbon source, because it is made of wood and intermediates Earth's carbon cycle. Laser ablation effects are compared to other carbon materials.

4.1. Hydrogen generation from carbon in water

During a trial of nanoparticle generation by laser ablation in the liquid phase, we found that bubbles rose from the irradiated site inside a bottle which contained powder of binchotan charcoal and water. After preliminary discovery of explosive combustion of the generated gas by ignition, the collected gas was analyzed to find that hydrogen gas was contained. **Table 1** shows the ratio of the generated gas components, where argon portion from the argon-purged water was excluded. In the collected gas, roughly 50% of hydrogen and 20% of carbon monoxide were contained, whereas the amount of oxygen was very low [20, 21]. No gas was generated from pure water itself under the same irradiation conditions. From these facts, it was concluded that the reaction is due to photochemical reaction of carbon with water, instead of ideal water-splitting. Alcohol additive enhanced the generated gas volume with 56% of hydrogen concentration [21] as shown in the third row in **Table 1**. Details are described in Section 4.3.

	H_2 (%)	O_2 (%)	CO (%)	CO_2 (%)	N_2 (%)	CH (%)
100% H_2O	48.7	1.3	20.5	0.5	5.1	23.1
50% EtOH/H_2O	56.2	2.7	25.2	0.0	5.5	8.5

In both rows, values show a ratio excluding the argon. Adapted with permission from Refs. [20, 21].

Table 1. Ratio of gas component obtained from binchotan suspension by laser irradiation under argon atmosphere with argon-purged water (100% H_2O) and 50 wt% ethanol/argon-purged water (50% EtOH/H_2O).

From the ratio of the generated gas components, the reaction resembles to that of coal gasification, which is a classical technique of syngas production by steaming of coal under high pressure (a few MPa) and high temperature (>800°C) (HPHT) [42] via the following:

$$C(s) + H_2O(g) \rightarrow H_2(g) + CO(g) \tag{1}$$

http://dx.doi.org/10.5772/64939

$$C(s) + 2H_2O(g) \rightarrow 2H_2(g) + CO_2(g) \quad (2)$$

$$3\,C(s) + O_2(g) + H_2O(g) \rightarrow H_2(g) + 3CO(g) \quad (3)$$

$$2\,C(s) + O_2(g) + 2H_2O(g) \rightarrow 2H_2(g) + 2CO_2(g) \quad (4)$$

$$2\,C(s) + 2H_2O(g) \rightarrow CH_4(g) + CO_2(g) \quad (5)$$

In the present laser-induced reaction, the water temperature rose from 22 to 29°C during the 30-min irradiation at 182 mJ/cm^2 for 9.5 mL volume of water. Further evidence of temperature elevation in the laser pulse duration was witnessed by optical emission spectroscopy as discussed later in Section 4.5.

4.2. Laser fluence dependence

The hydrogen-included gas was generated above a threshold fluence of nanosecond laser pulse irradiation. **Figure 7a** shows the laser fluence dependence of a generated gas volume after 30 min of irradiation at a laser wavelength of 532 nm for three kinds of carbon powders. Macroscopic gas volumes of more than 0.05 mL were detectable only above a laser fluence of ca. 50 mJ/cm^2. The gas volume generated with binchotan charcoal powder of 5 μm in diameter (A, red solid circles) was almost twice that of the high-grade carbon powder of 5 μm (B, black open circles) and graphite powder of less than 45 μm (C, blue solid triangles) under the same irradiation conditions, whereas the threshold laser fluences were nearly coincident. The generated gas volume increased by irradiation time within one hour, but the further prolonged

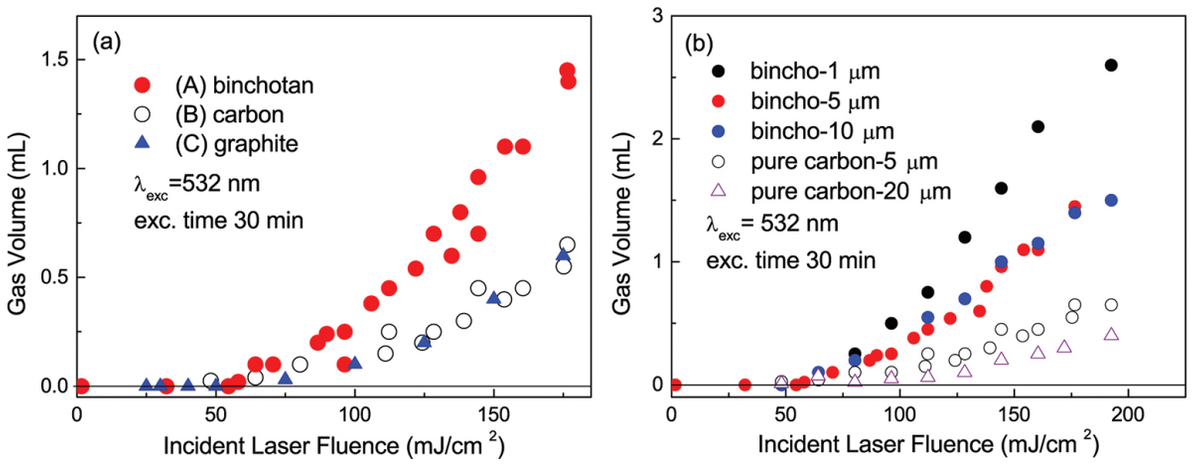

Figure 7. (a) Laser fluence dependence of generated gas volume with irradiation at 532 nm for 30 min, 26 mg of binchotan charcoal powder (A, red solid circles), high-grade carbon powder (B, black open circles), and graphite powder (C, blue solid triangles). The results for sample A and B were adapted with permission from Ref. [20]. (b) Laser fluence dependence of generated gas volume for powders of different sizes in diameter.

irradiation at 144 mJ/cm^2 made irreducible change, and the generated gas volume decreased [20]. This hydrogen generation reaction did not proceed by the irradiation of 30 fs laser pulses which affords a laser fluence of 80 mJ/cm^2 [20], implying the present reaction is classified into the thermal ablation process [1].

The BET surface area of the binchotan of 5 μm (A) was 22 ± 3 m^2/g, which was almost twice that of the high-grade carbon powder of 5 μm (B) 13 ± 3 m^2/g [20] or the graphite powder of less than 45 μm (C) 9 ± 3 m^2/g. Therefore, the higher gas generation is mainly attributed to its larger surface area. However, when the gas volume was compared to binchotan powders of different sizes of 1, 5, and 10 μm in mean diameter, whose BET surface areas were 120, 22, and 8 m^2/g, the generated volume did not depend on the surface area ratio linearly as shown in **Figure 7b**. This fact implies that there are other factors affecting the reaction efficiency.

The gas generation was observed from VIS to near-infrared (NIR) irradiation for both cases with binchotan (A) and pure carbon (B). **Figure 8** shows the generated gas volume versus the irradiated wavelength, obtained for 30 min irradiation at a laser fluence of 112 mJ/cm^2. The gas volume generated with binchotan (A, red solid circles) was more than twice that of the pure carbon (B, black open circles) under the same irradiation conditions in the VIS-NIR range. A tendency for a reduction in gas yield at longer wavelengths was anticorrelated to the optical reflectivity [20].

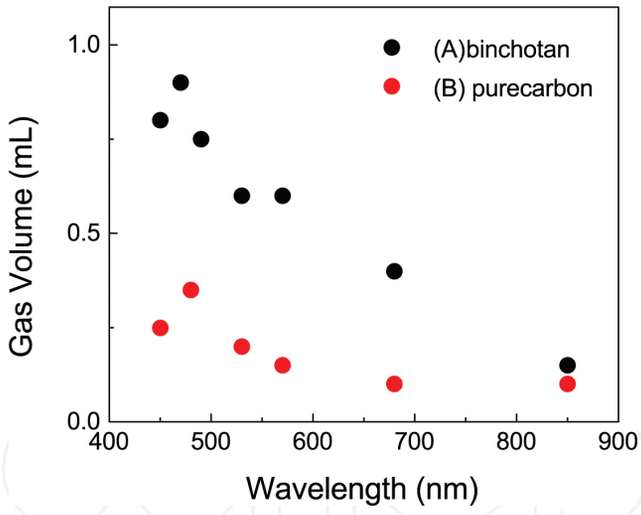

Figure 8. Irradiated wavelength dependence of the generated gas volume for binchotan powder (A, solid circles) and pure carbon powder (B, red circles) obtained by pulse irradiation of 112 mJ/cm^2 for 30 min. The result for sample A was adapted with permission from Ref. [20].

4.3. Alcohol additive effect

An alcohol additive in the binchotan water suspension enhanced the hydrogen generation efficiency for the laser fluences above the threshold of ca. 50 mJ/cm^2 [21]. Among methanol, ethanol, and isopropanol, ethanol was the most efficient additive and raised twice the generated volume. The generated volume increased according to the increase of ethanol additive

http://dx.doi.org/10.5772/64939

and saturated at 40–50% of ethanol in water. The generated gas contained 56% of hydrogen as shown in **Table 1**.

Alcohol is known to act as an oxygen scavenger preventing the reverse reaction into water [43, 44] and/or as a current doubler [45] in photocatalytic water splitting. As the present photochemical reaction is different from the photocatalytic water-splitting reaction, the enhancement of the reaction is partially due to a photochemical reaction of ethanol itself. Endothermic reactions of a steam reformation of ethanol, $C_2H_5OH + 3H_2O \rightarrow 2CO_2 + 6H_2$ and/or $C_2H_5OH + H_2O \rightarrow 2CO + 4H_2$, which usually progress under HPHT [40], might occur by the laser irradiation, in addition to the oxidation reactions of solid carbon.

The generated gas volume of 7.3 mL, which was obtained after 1 h of irradiation with a 209 mJ/pulse at 532 nm by the 50% ethanol additive [21], was quite small. According to the hydrogen ratio of 56%, the hydrogen amount included in the volume was calculated as 0.17 mmol. That is, one hydrogen molecule per 126 photons was generated, assuming that 64% of the irradiated laser power was used in the reaction [20]. Although this gas volume was comparable to the production by a photocatalytic water reduction with hydrogen-terminated nano-diamonds [30], it was much less than the carbon-assisted electrochemical hydrogen generation by electric power [46].

4.4. Nanoparticle generation

A post-irradiated solution was investigated using UV-VIS absorption and DLS methods. As shown in **Figure 9**, light extinction by UV absorption and light scattering appeared in the centrifuged solution following the irradiation. This change indicates the production of new materials by laser ablation as by-products of the hydrogen generation. DLS measurements showed that this solution contained nanoparticles of 125 nm in mean diameter (see the inset). Such nanoparticles could be measured only for the irradiation above the threshold fluence that is the same as that for gas generation. The mean diameter of the nanoparticles was independent

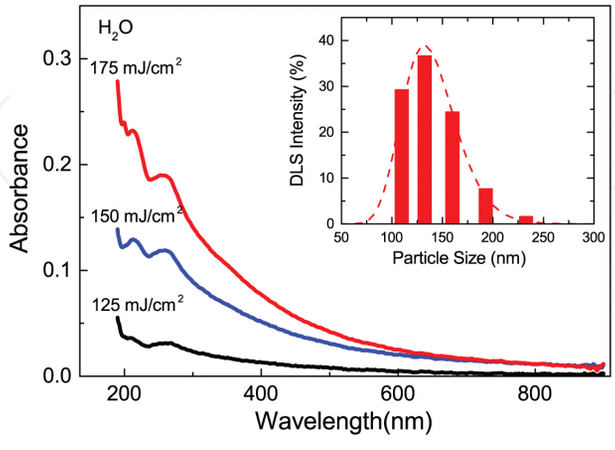

Figure 9. UV-Vis absorption spectra of centrifuged solutions after laser irradiation at 125 (black line), 150 (blue line), and 175 (red line) mJ/cm^2 for binchotan in water. Inset: size distribution of nanoparticles (bars) and logarithmic normal distribution function (broken line) in the centrifuged solution created by laser irradiation at 175 mJ/cm^2, measured using the DLS method. Adapted with permission from Ref. [36].

of the laser fluence, whereas light extinction was enhanced at higher irradiation fluences corresponding to an increase in the nanoparticle number. Furthermore, the generated nanoparticles are slightly dressed by a negative ζ-potential (−15 MeV) in water. Therefore, the nanoparticles suspended in water are expected to be stable for a long time as in the case of the organic QQ nanoparticles mentioned in Section 3.

A TEM image of the nanoparticles is shown in **Figure 10a**. Nanoparticles with sizes of around 100 nm were typically observed, as indicated by a yellow circle for a typical one. The sizes of the nanoparticles are consistent with the mean diameter observed by the DLS. A selected area electron diffraction (SAED) pattern of the nanoparticles (**Figure 10b**) shows clear diffraction spots in addition to diffused halo rings, whereas the Debye-Scherrer rings from the carbon structure were observed in a SAED pattern from the nonirradiated particle ensemble (**Figure 10c**). Some of spots in **Figure 10b** was located on the rings derived from the lattice spacings of diamond, and other parts of spots were on those of the C8 and n-diamond that were produced by laser ablation of a graphite target covered by water [29]. There were still other diffraction spots that could not be assigned to diffraction patterns of known structures. These results indicate that various crystalline/amorphous carbon structures including nanocrystalline carbon/diamond were created by laser ablation of binchotan charcoal in the liquid phase.

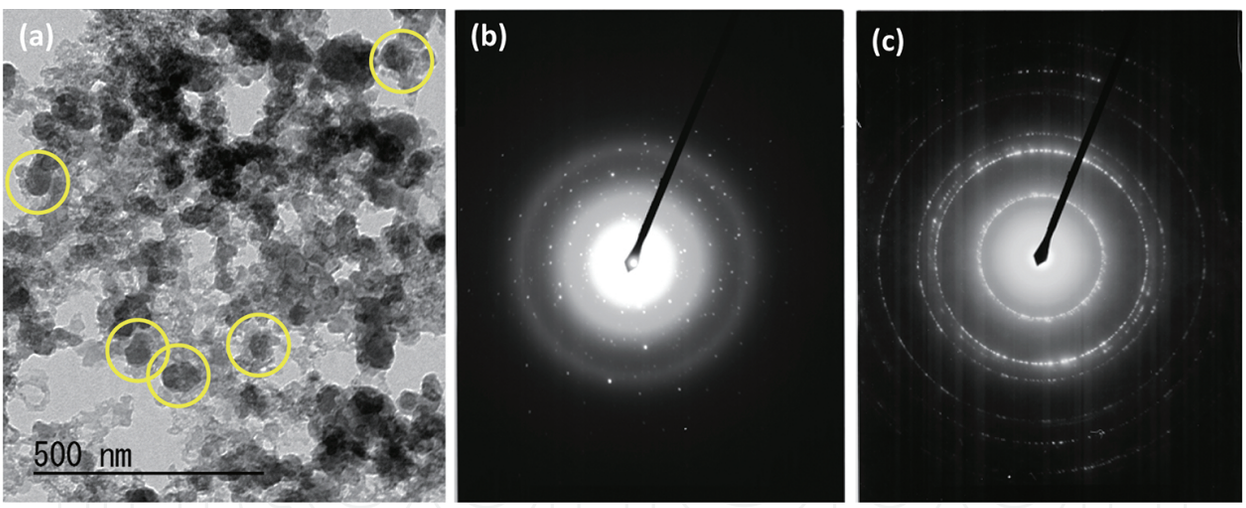

Figure 10. (a) A TEM image of binchotan nanoparticles produced by laser ablation. (b) SAED pattern obtained from the nanoparticles. (c) SAED pattern obtained from binchotan powder before irradiation.

Furthermore, the dried nanoparticles on a silicon substrate showed new IR peaks at 797, 873, 1019, 1261, 1425, 2906, and 2963 cm^{-1} as shown in **Figure 11**. Generally, vibrations of aromatic molecules are observed in the fingerprint range of 500–1500 cm^{-1}, and C—H stretch modes are in 2800–3000 cm^{-1} by an FT-IR measurement. The Raman peaks of O—H bonding were also observed during the reaction as described in Section 4.5. Therefore, the appearance of the peaks in these ranges indicated the creation of small carbon networks including the bonding of C—H and O—H groups.

http://dx.doi.org/10.5772/64939

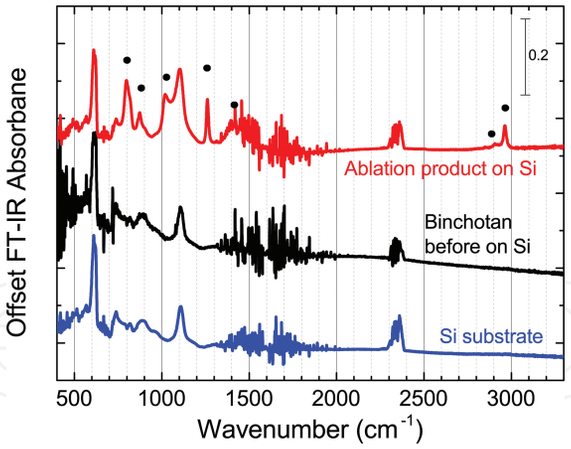

Figure 11. FT-IR spectra of dried post-irradiated nanoparticles (a red line) and nonirradiated binchotan powder (a black line) on a silicon substrate at room temperature. For comparison, the spectrum of a silicon substrate (a blue line) is also shown.

It is known that charcoal constitutes a form of amorphous carbons consisting of sp^2 and sp^3 bonding [47]. For the creation of new networks, bond breaking and reconstruction occur during the laser ablation by nanosecond pulses. Light energy at the threshold is necessary for such reactions. Surprisingly, in graphite powder, no nanoparticle was measured, and no additional IR peaks were observed.

4.5. Mechanism of the hydrogen generation

A clue to understand the mechanism behind the hydrogen generation via intense light irradiation is to clarify the nonequilibrium conditions at the irradiated site within a nanosecond time period. Investigation by time-integrated/-resolved spectroscopy during the hydrogen generation provided us crucial information regarding on-site nonequilibrium conditions including temperature increases [36].

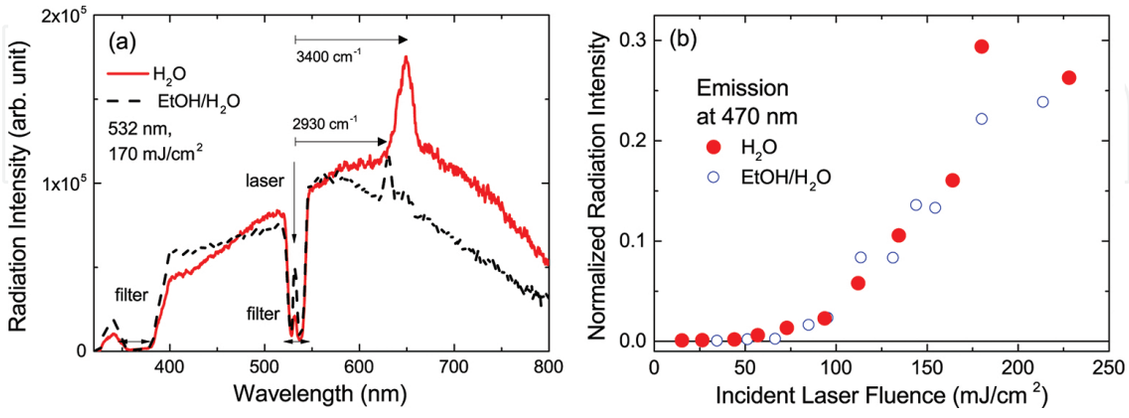

Figure 12. (a) Optical emission spectra from binchotan block in water (red solid line) and in 50% ethanol aqueous solution (broken black line) excited by laser pulses with 170 mJ/cm^2 energy density and 532 nm wavelength. (b) Incident laser fluence dependence of emission intensity at 470 nm for binchotan block in water (red solid circles) and in 50% ethanol aqueous solution (blue open circles). Adapted with permission from Ref. [36].

White-light emission was observed during the reaction from a binchotan block in water. As shown in **Figure 12a**, a broad spectrum over the visible range is apparent on both sides of the 532 nm excitation wavelength, across the penetration gap of the super notch filter, in water (solid red line), or in 50% ethanol aqueous solution (broken black line). No emission was observed from the water itself. The relatively narrow peaks at 650 and 630 nm are attributed to the Raman scattering lines at 3400 and 2930 cm^{-1}, because the peak positions changed following excitation wavelengths. There was no indication of the plasma emission from neutral/ionized atoms typically observed in LIBS. The Raman scattering lines are assigned to vibration of the O—H stretch mode under a hydrogen bond and Raman-active C—H vibrational modes of ethanol [48].

The white-light emission appeared only above a threshold excitation energy density. As shown in **Figure 12b**, the emission intensity at 470 nm increased nonlinearly in accordance with variations in the incident laser fluence. The threshold at 50 mJ/cm^2 was identical for both specimens in the water (red solid circles) and 50% ethanol aqueous solution (blue open circles). Note that the threshold for the appearance of the white light is coincident with the threshold for hydrogen generation (**Figure 7**). Therefore, it is reasonable to consider that the white-light emission is a simultaneous product of the hydrogen generation reaction. With a carbon electrode (99.9%), one fifth of emission intensity was observed above similar threshold excitation energy, and the generated gas volume was also small.

Spectral shape at shorter than 650 nm is well reproduced by Planck's law at a temperature 3860 K. Furthermore, time-resolved spectrum revealed a repetitive spectral change due to the temperature variation in the duration of laser pulse [36]. From these experimental facts, it was confirmed that the laser pulse supplies heat energy through optical absorption, and the white-light emission can reasonably be attributed to blackbody radiation from the irradiated site. It implies that hydrogen generation induced by laser irradiation proceeds similarly to classical coal gasification, which features reactions at HPHT. Finally, it was concluded that the hydrogen generation induced by the laser pulse irradiation occurs under high-pressure and high-temperature conditions.

5. Conclusion

The extended abilities of laser ablation in liquid phase were presented through two topics. The first is nanoparticle formation of an organic material, which produced a colloidal solution of a small organic material. In a yellow pigment QQ, a systematic blueshift of the absorption peak corresponding to the decrease of particle size in colloidal solutions was discoverd. This dependence provides an easy estimation method of the averaged diameter of the ensemble that will be applied to organic devices by a wet process. Furthermore, the population of an excited triplet state through optical excitation might be one guideline to select and synthesize materials for laser fragmentation.

The second is hydrogen gas generation from solid carbon in water by a photochemical reaction. Even under a lower energy irradiation that achieves no plasma state, the irradiated site

can be a reaction centre of energy conversion from light to a fuel gas, although the gas generation efficiency is very low. Simultaneously produced carbon-based nanoparticles possess a characteristic structure including those of diamond, nano-diamond, and diamond-like carbon, supplying new carbon materials from binchotan charcoal. A rise of temperature during the irradiated pulse duration was witnessed by the observation of white-light emission from the site ascribed to the blackbody radiation. Therefore, we conclude that the hydrogen generation induced by the laser pulse irradiation occurs under high-pressure and high-temperature conditions.

Laser ablation in the liquid phase is a useful technique to transform ordinary materials into functional ones under relatively mild condition. Although to date this technique has been applied to rather limited number of materials, further studies from various interests will extend the application field.

Acknowledgements

This work was supported by the Original Research Support Project of Wakayama University, 2011–2012. All experiments presented here were done with students of master's and bachelor's courses in Wakayama University from 2011 to 2016. TEM observations were performed under the Inter-university Cooperative Research Program of the Institute for Materials Research, Tohoku University. This publishing project was supported by the Kansai Research Foundation for technology promotion (2016P001).

Author details

Ikuko Akimoto* and Nobuhiko Ozaki

*Address all correspondence to: akimoto@sys.wakayama-u.ac.jp

Wakayama University, Sakaedani, Wakayama, Japan

References

[1] B. C. Stuart, M. D. Feit, S. Herman, A. M. Rubenchik, B. W. Shore, and M. D. Perry, Optical ablation by high-power short-pulse lasers, J. Opt. Soc. Am. B 1996, 13, 459-468.

[2] H. Zeng, X.-W. Du, S. C. Singh, S. A. Kulinich, S. Yang, J. He, and W. Cai, Nanomaterials via laser ablation/irradiation in liquid: A review, Adv. Funct. Mater. 2012, 22, 1333-1353.

[3] H. Fukuhara and H. Masuhara, The mechanism of dopant-induced laser ablation: Possibility of cyclic multiphotonic absorption in excited states, Chem. Phys. Lett. 1994, 221, 373-378.

[4] H. Fujiwara, H. Fukuhara, and H. Masuhara, Laser ablation of a pyrene-doped poly(methyl methacrylate) film: Dynamics of pyrene transient species by spectroscopic measurements, J. Phys. Chem. 1995, 99, 11844-11853.

[5] V. V. Volkov, T. Asahi, H. Masuhara, A. Masuhara, H. Kasai, H. Oikawa, and H. Nakanishi, Size-dependent optical properties of polydiacetylene nanocrystal, J. Phys. Chem. B 2004, 108, 7674-7680.

[6] Y. Tamaki, T. Asahi, and H. Masuhara, Tailoring nanoparticles of aromatic and dye molecules by excimer laser irradiation, Appl. Surf. Sci. 2000, 168, 85-88.

[7] Y. Tamaki, T. Asahi, and H. Masuhara, Nanoparticle formation of vanadyl phthalocyanine by laser ablation of its crystalline powder in a poor solvent, J. Phys. Chem. A 2002, 106, 2135-2139.

[8] Y. Tamaki, T. Asahi, and H. Masuhara, Solvent-dependent size and phase of vanadyl phthalocyanine nanoparticles formed by laser ablation of VOPc crystal-dispersed solution, Jpn. J. Appl. Phys. 2003, 42, 2725-2729.

[9] Y. Hosokawa, M. Yashiro, T. Asahi, and H. Masuhara, Photothermal conversion dynamics in femtosecond and picosecond discrete laser etching of Cu-phthalocyanine amorphous film analysed by ultrafast UV–VIS absorption spectroscopy, J. Photochem. Photobio. A: Chem. 2001, 142, 197-207.

[10] T. Sugiyama, T. Asahi, T. Takeuchi, and H. Masuhara, Size and phase control in quinacridone nanoparticle formation by laser ablation in water, Jpn. J. Appl. Phys. 2006, 45, 384-388.

[11] H.-G. Jeon, T. Sugiyama, H. Masuhara, and T. Asahi, Preparation and photoconductive property of electrophoretically deposited film of quinacridone nanoparticles prepared by laser ablation in water, Jpn. J. Appl. Phys. 2007, 46, L733-L735.

[12] T. Asahi, T. Sugiyama, and H. Masuhara, Laser fabrication and spectroscopy of organic nanoparticles, Acc. Chem. Resea. 2008, 41, 1790-1798.

[13] R. Yasukuni, T. Asahi, T. Sugiyama, H. Masuhara, M. Sliwa, J. Hofkens, F.C. De Schryver, M. van der Auweraer, A. Herrmann, and K. Muellen, Fabrication of fluorescent nanoparticles of dendronized perylenediimide by laser ablation in water, Appl. Phys. A 2008, 93, 5-9.

[14] R. Yasukuni, M. Sliwa, J. Hofkens, F.C. De Schryver, A. Herrmann, K. Muellen, and T. Asahi, Size-dependent optical properties of dendronized perylenediimide nanoparticle prepared by laser ablation in water, Jpn. J. of Appl. Phys 2009, 48, 065002 (6 pp).

[15] H. Tabata, M. Akamatsu, M. Fujii, and S. Hayashi, Formation of C_{60} colloidal particles suspended in poor solvent by pulsed laser irradiation, Jpn. J. Appl. Phys. 2007, 46, 4338-4343.

[16] L. V. Zhigilei and B. J. Garrison, Microscopic mechanisms of laser ablation of organic solids in the thermal and stress confinement irradiation regimes, J. Appl. Phys. 2000, 88, 1281-1297.

[17] C. W. Tang and S. A. VanSlyke, Organic electroluminescent diodes, Appl. Phys. Lett. 1987, 51, 913-915.

[18] H. Klauk, D. J. Gundlach, J. A. Nichols, and T. N. Jackson, Pentacene organic thin-film transistors for circuit and display applications, IEEE Trans. Electr. Dev. 1999, 46, 1258-1263.

[19] D. R. Gamota, P. Brazis, K. Kalyanasundaram, J. Zhang, Printed Organic and Molecular Electronics, Springer Science & Business Media, 2013, Chapter 1 and 3.

[20] I. Akimoto, K. Maeda, and N. Ozaki, Hydrogen generation by laser irradiation of carbon powder in water, J. Phys. Chem. C 2013, 117, 18281-18285.

[21] K. Maeda, N. Ozaki, and I. Akimoto, Alcohol additive effect in hydrogen generation from water with carbon by photochemical reaction, Jpn. J. Appl. Phys. 2014, 53, 05FZ03 (3 pp).

[22] A. M. Squires, Clean fuels from coal gasification, Science 1974, 184, 340-346.

[23] A. Fujishima and K. Honda, Electrochemical photolysis of water at a semiconductor electrode, Nature 1972, 238, 37-38.

[24] T. Kawai and T. Sakata, Hydrogen evolution from water using solid carbon and light energy, Nature 1979, 282, 283-284.

[25] S. Sato and J. M. White, Photocatalytic reaction of water with carbon over platinized titania, J. Phys. Chem. 1981, 85, 336-341.

[26] T.-F. Yeh, J.-M. Syu, C. Cheng, T.-H. Chang, and H. Teng, Graphite oxide as a photocatalyst for hydrogen production from water, Adv. Funct. Mater. 2010, 20, 2255-2262.

[27] H.-C. Hsu, I. Shown, H.-Y. Wei, Y.-C. Chang, H.-Y. Du, Y.-G. Lin, C.-A. Tseng, C.-H. Wang, L.-C. Chen, Y.-C. Lind, and K.-H. Chen, Graphene oxide as a promising photocatalyst for CO_2 to methanol conversion, Nanoscale, 2013, 5, 262-268.

[28] I. Shown, H.-C. Hsu, Y.-C. Chang, C.-H. Lin, P. K. Roy, A. Ganguly, C.-H. Wang, J.-K. Chang, C.-I. Wu, L.-C. Chen, and K.-H. Chen, Highly efficient visible light photocatalytic reduction of CO_2 to hydrocarbon fuels by Cu-nanoparticle decorated graphene oxide, Nano Lett. 2014, 14, 6097-6103.

[29] S. Z. Mortazavi, P. Parvin, A. Reyhani, S. Mirershadi, and R. Sadighi-Bonabi, Generation of various carbon nanostructures in water using IR/UV laser ablation, J. Phys. D: Appl. Phys. 2013, 46, 165303 (9 pp).

[30] D. M. Jang, Y. Myung, H. S. Im, Y. S. Seo, Y. J. Cho, C. W. Lee, J. Park, A.-Y. Jee, and M. Lee, Nanodiamonds as photocatalysts for reduction of water and graphene oxide, Chem. Comm. 2012, 48, 696-698.

[31] A. A. Voevodin and M. S. Donley, Preparation of amorphous diamond-like carbon by pulsed laser deposition: a critical review, Surf. Coat. Tech. 1996, 82, 199-213.

[32] M. Capitelli, A. Casavola, G. Colonna, and A. De Giacomo, Laser-induced plasma expansion: theoretical and experimental aspects, Spectrochimica Acta Part B 2004, 59, 271-289.

[33] L. J. Radziemski, T. R. Loree, D. A. Cremers, and N. M. Hoffman, Time-resolved laser-induced breakdown spectrometry of aerosols, Anal. Chem. 1983, 55, 1246-1252.

[34] I. Akimoto, M. Ohata, N. Ozaki, and G. Ping, Formation of nanoparticles of organic molecules by liquid laser ablation, MRS Proceedings. 2012, 1455: mrss12-1455-ii08-04 (6 pp), (DOI: 10.1557/opl.2012.1346).

[35] I. Akimoto, M. Ohata, N. Ozaki, and P. Gu, Size dependent optical properties of quinacridonequinone nanoparticles prepared by liquid laser ablation in water, Chem. Phys. Lett. 2012, 552, 102-107.

[36] I. Akimoto, S. Yamamoto, and K. Maeda, White-light emission from solid carbon in aqueous solution during hydrogen generation induced by nanosecond laser pulse irradiation, Appl. Phys. A 2016, 122, 675 (6 pp).

[37] S. Kita, S. Masuo, S. Machida, and A. Itaya, Nanoparticle formation of pentacene by laser irradiation in ethanol solution, Jpn. J. Appl. Phys. 2006, 45, 6501-6507.

[38] H. Nishi, Chemistry of quinacridone, Seisan-kenkyu 1965, 17, 159-169 (in Japanese).

[39] M. Vilkman, T. Hassinen, M. Keranen, R. Pretot, P. van der Schaaf, T. Ruotsalainen, H. G. O. Sandberg, Fully roll-to-roll processed organic top gate transistors using a printable etchant for bottom electrode patterning, Org. Electron. 2015, 20, 8-14.

[40] M. S. Dresselhaus, G. Dresselhaus, and P. C. Eklund, Science of Fullerenes and Carbon Nanotubes, Academic Press, 1996, Chapter 13.

[41] I. Akimoto and K. Kan'no, Photoluminescence and near-edge optical absorption in the low-temperature phase of pristine C_{60} single crystals, J. Phys. Soc. Jpn. 2002, 71, 630-643.

[42] L. M. Gandia, G. Arzamendi, and P. M. Dieguez, editors, Renewable Hydrogen Technologies: Production, Purification, Storage, Applications and Safety, Elsevier, Amsterdam. 2013, Chaps. 6 and 7.

[43] T. Kawai and T. Sakata, Photocatalytic hydrogen production from liquid methanol and water, J. Chem. Soc.: Chem. Commun. 1980, 694-695, (DOI: 10.1039/C39800000694).

[44] Michael Bowker, Sustainable hydrogen production by the application of ambient temperature photocatalysis, Green Chem. 2011, 13, 2235-2246.

[45] S. R. Morrison and T. Freund, Chemical role of holes and electrons in ZnO photocatalysis, J. Chem. Phys. 1967, 47, 1543-1551.

[46] M. S. Seehra, S. Bollineni, Nanocarbon boosts energy-efficient hydrogen production in carbon-assisted water electrolysis, Int. J. Hydrogen Energy, 2009, 34, 6078-6084.

[47] K. Ishimaru, T. Hata, P. Bronsveld, T. Nishizawa, and Y. Imamura, Characterization of sp^2- and sp^3-bonded carbon in wood charcoal, J. Wood Sci. 2007, 53, 442-448.

[48] A. D'Aprano, A. Lizzio, V. T. Liveri, F. Aliotta, C. Vasi, and P. Migliardo, Aggregation states of water in reversed AOT micelles: Raman evidence, J. Phys. Chem. 1988, 92, 4436-4439.

IntechOpen